

the basis of their Voyager 1 measurements, Warwick *et al.* (20) and Kaiser *et al.* (21) conclude that the source of the strongest Saturnian kilometric radiation is located in the northern hemisphere. If there is a connection between such radiation and the particle dropouts, it may not be surprising that the dropouts were not observed by Voyager 2 since the outbound trajectory was in the southern hemisphere.

The north-south asymmetry in Saturnian kilometric radiation calls to mind the asymmetric electron pitch-angle distributions (Fig. 5), which represented a deficiency of ~ 60- to 200-keV electrons returning from the southern high latitude regions. Why were they not measured by Voyager 1? Comparing Fig. 7, A and B, we see that wherever Voyager 2 saw asymmetric pitch-angle distributions, inbound or outbound, Voyager 1 saw bidirectional cigar-shaped distributions. Thus the Voyager 1 cigar distributions may be manifestations of the same source, but with different boundary conditions near the polar regions.

In summary, if we allow for plausible differences in the dynamic state of Saturn's magnetosphere, the Voyager 1 and Voyager 2 energetic particle measurements complement each other and lead to a reasonably consistent global picture of a novel magnetosphere.

S. M. KRIMIGIS
Applied Physics Laboratory,
Johns Hopkins University,
Laurel, Maryland 20707

T. P. ARMSTRONG
Department of Physics, University of
Kansas, Lawrence 66044

W. I. AXFORD
Max-Planck Institute for Aeronomy,
D-3411 Katlenburg-Lindau 3,
West Germany

C. O. BOSTROM
Applied Physics Laboratory,
John Hopkins University

G. GLOECKLER
Department of Physics and Astronomy,
University of Maryland, College Park

E. P. KEATH
Applied Physics Laboratory,
Johns Hopkins University

L. J. LANZEROTTI
Bell Laboratories,
Murray Hill, New Jersey 07974

J. F. CARBARY
Applied Physics Laboratory,
Johns Hopkins University

D. C. HAMILTON
Department of Physics and Astronomy,
University of Maryland

E. C. ROELOF
Applied Physics Laboratory,
Johns Hopkins University

References and Notes

- S. M. Krimigis, T. P. Armstrong, W. I. Axford, C. O. Bostrom, C. Y. Fan, G. Gloeckler, L. J. Lanzerotti, *Space Sci. Rev.* **21**, 329 (1977).
- S. M. Krimigis, J. F. Carbary, E. P. Keath, C. O. Bostrom, W. I. Axford, G. Gloeckler, L. J. Lanzerotti, T. P. Armstrong, *J. Geophys. Res.* **86**, 8227 (1981).
- S. M. Krimigis *et al.*, *Science* **212**, 225 (1981).
- J. A. Simpson, T. S. Bastian, D. L. Chenette, R. B. McKibben, K. R. Pyle, *J. Geophys. Res.* **85**, 5731 (1980).
- J. A. Van Allen, B. A. Randall, M. F. Thomsen, *ibid.*, p. 5679.
- F. B. McDonald, A. W. Schardt, J. H. Trainor, *ibid.*, p. 5813.
- W. Fillius and C. E. McIlwain, *ibid.*, p. 5803.
- S. M. Krimigis *et al.*, *Science* **206**, 977 (1979).
- S. M. Krimigis *et al.*, conference on "Physics of the Jovian and Saturnian Magnetospheres," Applied Physics Laboratory, Johns Hopkins University, Laurel, Md., 22 to 24 October 1981.
- L. A. Frank, B. G. Burek, K. L. Ackerson, J. H. Wolfe, J. D. Mihalov, *J. Geophys. Res.* **85**, 5695 (1980).
- D. C. Hamilton *et al.*, *Geophys. Res. Lett.* **7**, 813 (1980).
- E. C. Sittler, Jr., J. D. Scudder, H. S. Bridge, *Nature (London)* **292**, 711 (1981).
- A. Cheng, L. J. Lanzerotti, V. Pirronello, in preparation.
- H. S. Bridge *et al.*, *Science* **212**, 217 (1981).
- D. A. Gurnett, W. S. Kurth, F. L. Scarf, *ibid.*, p. 235.
- D. A. Gurnett and F. L. Scarf, in *Physics of the Jovian Magnetosphere*, A. Dessler, Ed. (Cambridge Univ. Press, Cambridge, in press).
- W. Fillius, in *Jupiter*, T. Gehrels, Ed. (Univ. of Arizona Press, Tucson, 1976), pp. 896-927.
- S. M. Krimigis and E. C. Roelof, in *Physics of the Jovian Magnetosphere*, A. Dessler, Ed. (Cambridge Univ. Press, Cambridge, in press).
- R. E. Johnson, L. J. Lanzerotti, W. L. Brown, T. P. Armstrong, *Science* **212**, 1027 (1981).
- J. W. Warwick *et al.*, *ibid.*, p. 239.
- M. L. Kaiser, M. D. Desch, A. Lacacheux, *Nature (London)* **292**, 731 (1981).
- N. F. Ness, M. H. Acuña, R. P. Lepping, J. E. P. Connerney, K. W. Behannon, L. F. Burlaga, F. M. Neubauer, *Science* **215**, 558 (1982).
- We thank the Voyager Project Office, JPL, and the Planetary Programs Office, NASA Headquarters, for help and cooperating in carrying out this experiment. We thank D. P. Peletier, S. A. Gary, R. G. King, J. W. Kohl, D. E. Fort, J. T. Mueller, J. H. Crawford, R. E. Thompson, B. A. Northrop, and J. Hook at APL/JHU; E. O. Tums, J. C. Cain, R. T. Cates, R. A. Lundgren, and D. C. Brown of the University of Maryland; C. G. MacLennan of Bell Laboratories; and J. O'Donnell, S. T. Brandon, and M. Paonessa of the University of Kansas for their enthusiasm and long hours that made the LECF experiment a success. The work of E. Franzgrote, O. Diver, and D. Griffith of JPL (among many others) was essential to the success of our investigation. We thank N. F. Ness and the MAG team for making their data available before publication. The LECF program was supported at APL/JHU by NASA under task I of contract N00024-78-C-5384 between Johns Hopkins University and the Department of the Navy and by subcontract at the universities of Kansas and Maryland.

10 November 1981

Energetic Charged Particles in Saturn's Magnetosphere: Voyager 2 Results

Abstract. Results from the cosmic-ray system on Voyager 2 in Saturn's magnetosphere are presented. During the inbound pass through the outer magnetosphere, the ≥ 0.43 -million-electron-volt proton flux was more intense, and both the proton and electron fluxes were more variable, than previously observed. These changes are attributed to the influence on the magnetosphere of variations in the solar wind conditions. Outbound, beyond 18 Saturn radii, impulsive bursts of 0.14- to > 1.0 -million-electron-volt electrons were observed. In the inner magnetosphere, the charged particle absorption signatures of Mimas, Enceladus, and Tethys are used to constrain the possible tilt and offset of Saturn's internal magnetic dipole. At ~ 3 Saturn radii, a transient decrease was observed in the electron flux which was not due to Mimas. Characteristics of this decrease suggest the existence of additional material, perhaps another satellite, in the orbit of Mimas.

The Saturn encounter trajectory of Voyager 2 provided a novel perspective from which to study the structure and dynamics of the Saturnian magnetosphere. Although Voyager 2, Voyager 1, and Pioneer 11 all entered the magnetosphere near the noon meridian, the Voyager 2 entry was at a latitude of 17° , significantly higher than either of the other spacecraft. As it approached Saturn, Voyager 2 traveled to $\sim 30^\circ$ latitude at 4 Saturn radii (R_S , $1 R_S = 60,330$ km) before descending through the ring plane within the orbit of Mimas at $2.77 R_S$. Outbound, the spacecraft left Saturn near the dawn meridian at a local time similar to that traversed by Pioneer 11 but at -30° latitude. The large latitude range and the close approach to Saturn are among the unique features of this trajectory which were exploited in this

study of data obtained by the cosmic-ray system (1).

The outer magnetosphere. Voyager 2 entered Saturn's magnetosphere during a disturbed period when the solar wind pressure was highly variable (2). The fluxes of both energetic protons and electrons (Fig. 1) rose sharply ~ 15 minutes before the magnetopause crossing at $18.5 R_S$ (2, 3). Perhaps this precursor in the particle flux was related to the high latitude of the crossing or to magnetopause motion which may have kept Voyager 2 in the vicinity of the magnetopause for 15 minutes before the spacecraft finally crossed that boundary. Just inside the magnetosphere, the proton and electron intensities, and changes in these intensities, resembled those measured by Voyager 1 (4); however, starting at 0920 spacecraft event time (SCET)

on 25 August (day 237), at a distance of $16.5 R_S$, the ≥ 0.43 -MeV proton flux observed on Voyager 2 suddenly increased by an order of magnitude and became much more variable than the Voyager 1 flux at similar energies and distances. This disturbance lasted until 1630, day 237 ($\sim 11 R_S$) and was accompanied by fluctuations in the magnetic field (5). The factor of ~ 40 decrease at $15.5 R_S$ [corresponding to a magnetic L coordinate of ~ 17 (6)], is visible in both the proton and electron fluxes displayed in Fig. 1. It was suggested (4) that similar decreases observed outbound beyond $L = 10$ on Voyager 1 at a latitude of $\sim 20^\circ$ in the predawn direction resulted from variations in the solar wind pressure. Thus these Voyager 2 observations support earlier interpretations (4, 7) that solar wind conditions have a major influ-

ence on the energetic particle fluxes in the outer magnetosphere. They further suggest that this effect may be stronger at higher latitudes.

The ≥ 0.43 -MeV proton flux reached a plateau between $L = 15$ and $L = 11$ and then started decreasing toward the orbit of Rhea ($L = 8.8$) and the "slot" region ($L = 7.5$ to 4) (7). Despite the higher latitude of the Voyager 2 trajectory, the ≥ 0.43 -MeV proton flux at $L = 15$ was an order of magnitude higher than the Voyager 1 flux at the same L , and was comparable to the peak Voyager 1 flux observed inbound at $L = 10$.

During the outbound pass in the dawn direction at -29° latitude, both proton and electron fluxes decreased relatively smoothly out to $\sim 18 R_S$, except for several decreases lasting less than a few minutes in the ≥ 0.43 -MeV proton flux.

The proton flux showed only minor variations beyond $15 R_S$ and reached interplanetary values near $25 R_S$. In contrast, the 0.14- to 0.40-MeV electron flux remained well above interplanetary values (Figs. 1 and 2) and was highly variable beyond $18 R_S$. The time-intensity profiles of the events observed in this region suggest an impulsive injection and exponential decay of the electron flux. In general, a small magnetic field depression or increased field fluctuations accompanied the injections (5). These events, which were visible only in the energetic electron flux, were observed throughout the outer dawnside region from 18 to $70 R_S$.

Figure 2b shows an event observed at 1336 on 27 August. In this case, the injection occurred in two stages, separated by 7 minutes. The rise time of the

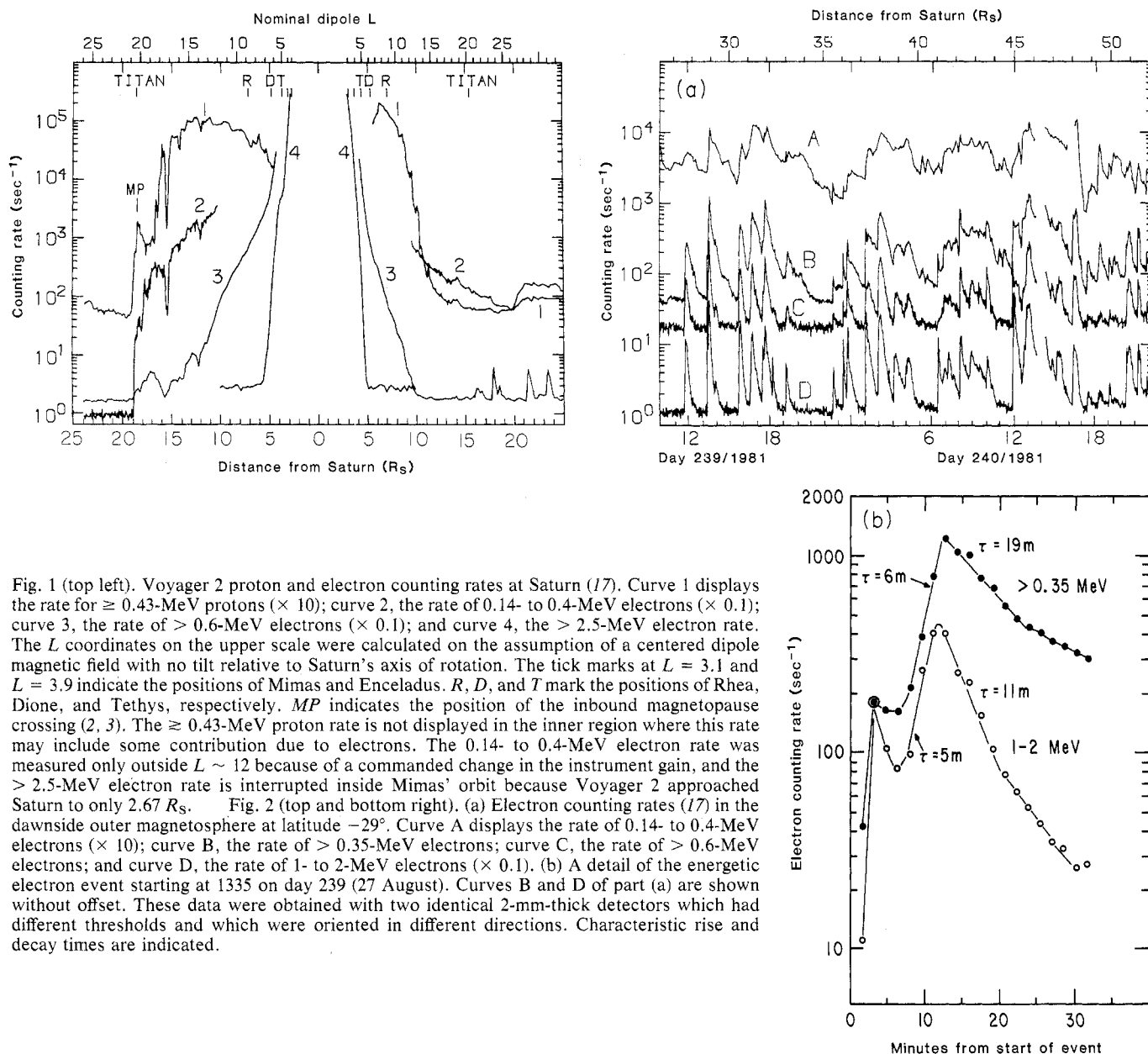


Fig. 1 (top left). Voyager 2 proton and electron counting rates at Saturn (17). Curve 1 displays the rate for ≥ 0.43 -MeV protons ($\times 10$); curve 2, the rate of 0.14- to 0.4-MeV electrons ($\times 0.1$); curve 3, the rate of > 0.6 -MeV electrons ($\times 0.1$); and curve 4, the > 2.5 -MeV electron rate. The L coordinates on the upper scale were calculated on the assumption of a centered dipole magnetic field with no tilt relative to Saturn's axis of rotation. The tick marks at $L = 3.1$ and $L = 3.9$ indicate the positions of Mimas and Enceladus. R , D , and T mark the positions of Rhea, Dione, and Tethys, respectively. MP indicates the position of the inbound magnetopause crossing (2, 3). The ≥ 0.43 -MeV proton rate is not displayed in the inner region where this rate may include some contribution due to electrons. The 0.14- to 0.4-MeV electron rate was measured only outside $L \sim 12$ because of a commanded change in the instrument gain, and the > 2.5 -MeV electron rate is interrupted inside Mimas' orbit because Voyager 2 approached Saturn to only $2.67 R_S$. Fig. 2 (top and bottom right). (a) Electron counting rates (17) in the dawnside outer magnetosphere at latitude -29° . Curve A displays the rate of 0.14- to 0.4-MeV electrons ($\times 10$); curve B, the rate of > 0.35 -MeV electrons; curve C, the rate of > 0.6 -MeV electrons; and curve D, the rate of 1- to 2-MeV electrons ($\times 0.1$). (b) A detail of the energetic electron event starting at 1335 on day 239 (27 August). Curves B and D of part (a) are shown without offset. These data were obtained with two identical 2-mm-thick detectors which had different thresholds and which were oriented in different directions. Characteristic rise and decay times are indicated.

larger increase was 5 to 6 minutes. The decay time was clearly energy dependent, and was ~ 19 minutes near 0.35 MeV and ~ 11 minutes for 1- to 2-MeV electrons. Most of the injection events appear to be quite similar, with an almost simultaneous rise at energies between 0.35 MeV and 1 to 2 MeV and decay times of 10 to 40 minutes, with the higher energy flux decaying faster. No regular periodicity is evident in these events; however, the typical time between successive events was 30 to 70 minutes.

It is significant that fluxes of electrons with such different energies peaked almost simultaneously. Such time coincidence is only possible if the electrons that we observed were accelerated on or very near to field lines passing through the spacecraft. Since the direction of the magnetic field observed throughout this region was roughly parallel to Saturn's equatorial plane, consistent with the sweeping-back of field lines to form the magnetotail (3), these electrons may have been accelerated in the magnetotail and then propagated along the field to the dawn meridian where they were observed. Also, since these events were observed to have such similar characteristics throughout this region, it is likely that the acceleration was occurring throughout a large spatial region, perhaps across the magnetotail, and that the discrete events that were observed re-

sulted from discrete, impulsive accelerations of these electrons rather than from spatial variations.

The inner magnetosphere. As observed during previous Saturn encounters (4, 7-10), the electron flux continued to increase through the slot region, reaching a maximum in the inner magnetosphere. The energy spectrum of the electrons that we observed became harder with decreasing L . The electron flux at energies below several million electron volts does not show the deep, long-term absorption effects of the inner moons of Saturn, the macroabsorption features; only microabsorption features are observed, and then only when the spacecraft passes the moon's orbit close to the longitude of the moon (4, 8-11).

The energetic proton fluxes observed in the inner magnetosphere ($L < 6$) are shown in Fig. 3. These fluxes were calculated from counting rates which have been corrected for accidental coincidences and dead time effects. These corrections were small outside the orbit of Mimas but they became large inside, where accidental coincidences amounted to 40 to 50 percent of the observed counting rates and only 10 to 15 percent of the incident particles were counted. Our preliminary results for the maximum proton fluxes observed on Voyager 2 at $2.75 R_S$ are 560 and 920 $\text{cm}^{-2} \text{sec}^{-1} \text{sr}^{-1}$ for the energy intervals 63 to 160 MeV

and 48 to 160 MeV, respectively. The flux of protons > 80 MeV reported at this distance by Pioneer 11 investigators (8, 10) was in the range of 900 to 1200 $\text{cm}^{-2} \text{sec}^{-1} \text{sr}^{-1}$. In view of the uncertainties associated with the effects of the angular distributions of these protons and the absolute calibrations of these different detector systems, these data may be consistent with no significant change in intensity during the 2-year interval between the Pioneer 11 and Voyager 2 encounters.

Absorption regions (macroabsorption signatures) at the orbits of Enceladus and Mimas are clearly visible in Fig. 3. The considerable width of the Mimas absorption region in the high-energy protons, the Mimas gap, is due to the large orbital eccentricity of Mimas. Further analysis is needed to identify the particles responsible for the residual flux in the Mimas gap, but the 63- to 160-MeV proton flux decreased in the gap by a factor of over 2000. With further analysis, this factor will yield an upper limit on the radial diffusion coefficient for the high-energy protons in this region.

The absorption effect of the G ring was observed at $L = 2.8$ during the outbound pass (Fig. 3). The much larger decrease apparent inbound near $L = 2.8$, just before the maximum in the proton flux, occurred during a spacecraft roll. The minimum of this decrease occurred when

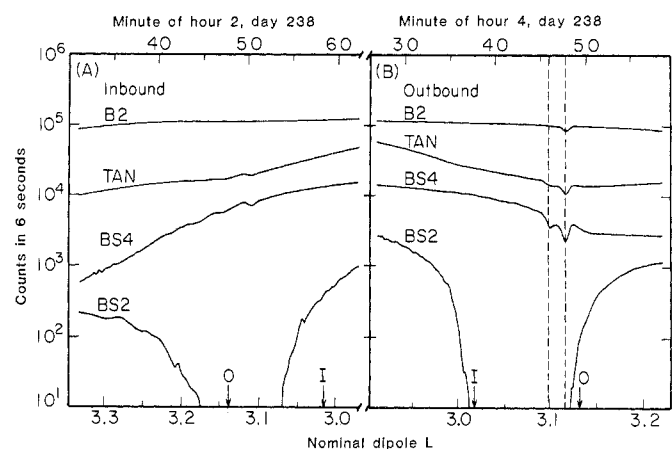
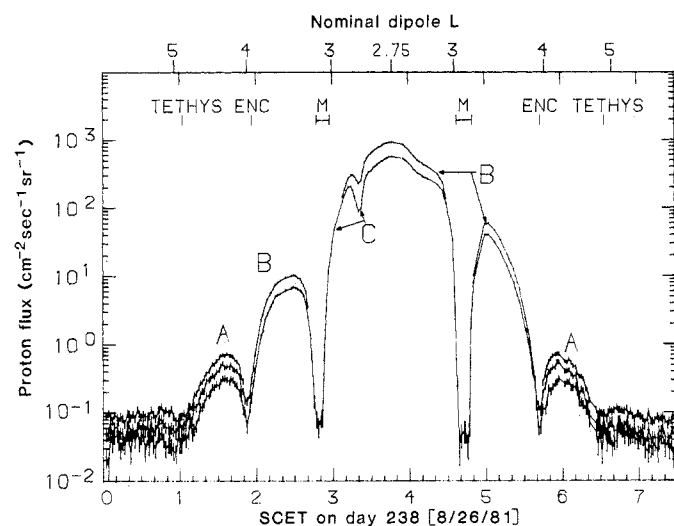


Fig. 3 (left). The energetic proton flux in the inner magnetosphere. Curve A displays the flux of 27- to 160-MeV protons and is not shown within $L = 4$ because of electron contamination in this rate. Curves B and C display the proton flux in the energy intervals 48 to 160 MeV and 63 to 160 MeV, respectively. Curve B is not displayed in the Mimas gap where the correction factors required to calculate this flux were unreliable. The L scale and the satellite positions were calculated on the assumption of a centered dipole magnetic field aligned with Saturn's axis of rotation. ENC and M indicate the orbits of Enceladus and Mimas. The sharp dip inside the orbit of Mimas inbound just before the peak flux was due to a spacecraft roll. The shoulder just after the peak flux reflects absorption of these protons by the G ring. The inbound G ring signature was obscured by the roll. Fig. 4 (right). Counting rates of four detector configurations versus L during the inbound (A) and outbound (B) passages across the orbit of Mimas. The time scale (SCET) is shown at the top of the figure. BS2 labels a fourfold coincidence rate corresponding to > 63 -MeV protons. The large decrease in this rate is due to absorption by Mimas. BS4 labels a twofold coincidence rate between detectors with nominal thresholds of 2.2 MeV and 5.3 MeV. In this region this rate is dominated by accidental electron coincidences. TAN labels a counting rate of a shielded detector which responds to > 3 -MeV electrons (with some response down to ~ 1 MeV). The B2 curve shows the response of a nearly unshielded detector with a 2.2-MeV threshold. This rate may include a substantial contribution from the pile-up of lower energy electrons. The expected L coordinates of the outer, O, and inner, I, edges of the Mimas absorption region are based on a centered, untilted dipole model of Saturn's magnetic field. The vertical dashed lines in (B) indicate a microabsorption signature due to an object in the approximate orbit of Mimas. As described in the text, Mimas was not responsible for this signature.

the acceptance cone of the instrument rolled through the direction nearly parallel to the magnetic field. Thus the pitch angle distribution of these protons had a minimum along the field direction. If the equatorial pitch angle distribution of these particles is of the form $\sin^n(\theta)$, then the value of n can be calculated at $L = 3.5$ from the flux ratio between the inbound (24° latitude) and outbound (-11° latitude) passes. Our value of $n \sim 6$ is somewhat larger than the $n \sim 4$ deduced by Van Allen *et al.* (10).

A microabsorption signature near Mimas. During the outbound passage of Voyager 2 through the Mimas gap ($L = 3.02$ to 3.14), a transient decrease was observed in the local electron flux at 0445 to 0449 SCET (Fig. 4B). The similarity between this feature and microabsorption signatures attributable to other satellites of Saturn (4, 7-11) suggests that it resulted from the absorption of electrons by material in the orbit of Mimas. No absorption feature of comparable or greater magnitude was observed in these rates during the spacecraft's passage inbound through this region (Fig. 4A), although in the higher energy TAN and BS4 rates several smaller fluctuations were observed. As we will demonstrate, these data are not consistent with the assumption that Mimas produced the outbound signature. Alternatively, they can be understood if another absorber is assumed to be at a longitude much nearer to the spacecraft than was Mimas. Thus there is probably additional material, perhaps a small satellite, sharing the orbit of Mimas.

The longitude relative to Mimas of the inbound and outbound legs of the Voyager 2 trajectory across the orbit of Mimas and the longitudinal drift rate of electrons relative to Mimas can be used to determine the conditions under which Mimas could have produced the observed signature. At 0448 SCET, when the outbound absorption signature was observed, Voyager 2 was at a longitude (Saturn longitude system, SLS) (12) of 337° and Mimas was 147° west of the spacecraft (that is, clockwise as viewed from the north) at 124° . Inbound, Voyager 2 crossed the orbit of Mimas at 321° SLS when Mimas was at 89° SLS, 128° west of the spacecraft. Assuming that Mimas was the absorbing body responsible for this signature, the time elapsed since absorption of these electrons by Mimas, the "age of the hole," can be calculated from this difference in longitude, the average angular velocity of Mimas, Saturn's rotation period, and the energy- and pitch-angle-dependent angular drift velocity of the electrons in Saturn's magnetic field. The result-

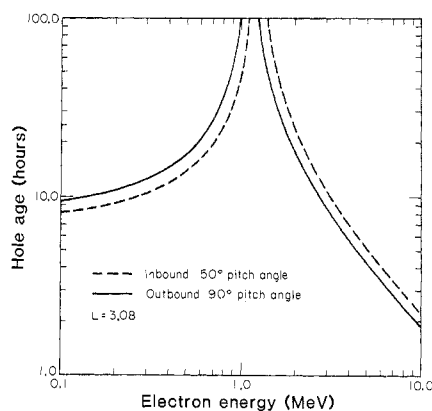


Fig. 5. The elapsed time between the formation of an absorption feature (hole) in the electron population and its observation at Voyager 2 plotted against electron energy, assuming Mimas is the absorbing body at a mean radial distance corresponding to $L = 3.08$. Curves for both the inbound and outbound trajectories are shown for the equatorial pitch angles which mirror at the latitude of the spacecraft. Rigid corotation of the magnetosphere was assumed in this calculation.

ant "hole age" is displayed in Fig. 5.

If one assumes that Mimas had produced the outbound absorption signature, the calculation for the hole age (Fig. 5) provides two important predictions concerning the characteristics of the absorption signature which are inconsistent with our observations. First, except near the ~ 1.1 MeV resonance energy, where the electron drift velocity

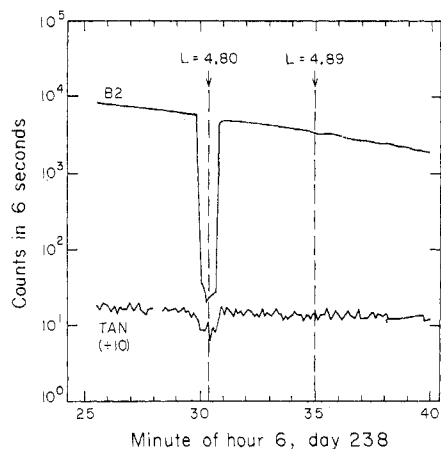


Fig. 6. Counting rates of electrons in nearly unshielded (B2) and shielded (TAN) detectors plotted against SCET near the orbit of Tethys as the spacecraft passed within 1° longitude of that satellite. The width of the absorption feature at 0630 corresponds to ~ 1100 km which is nearly equal to the 1050-km diameter of Tethys. The vertical dashed lines show the expected ($L = 4.89$) and observed ($L = 4.80$) coordinates of the absorption feature as calculated from a centered, untilted dipole model of Saturn's magnetic field. If the effect of the ring current suggested by Voyager 1 observations (8) had been included in this calculation, the absorption feature would have been expected at 0632 (16).

is equal to the orbital velocity of Mimas, the required hole age inbound would have differed from the outbound age by < 20 percent. The energy dependence of the electron drift velocity causes any absorption feature observed with a detector sensitive to a broad energy range to refill by an amount that is inversely proportional to the age of the hole. Thus, if Mimas had produced the outbound signature, a signature of similar depth should have been observed in the inbound data. As shown in Fig. 4, in each rate the outbound signature is more than twice as deep as any of the features observed inbound. Thus the absence of a similar signature inbound argues that the signature observed outbound could not have been due to Mimas.

Another satellite, however, close to the outbound longitude of the spacecraft, could produce a signature that was much deeper outbound than inbound, because any object orbiting Saturn at $L = 3.1$ which was east of the spacecraft would have been $\sim 20^\circ$ closer to the spacecraft in longitude during the outbound pass than it would have been inbound, and because the hole age is proportional to this longitude difference. For example, if the new satellite were 20° east of the spacecraft on the outbound pass, and hence 40° east on the inbound pass, inbound the signature would have been twice as old as outbound. If the object were even closer to the spacecraft outbound, the ratio of the hole ages inbound to outbound and hence the ratio of the depths of the signatures outbound to inbound would be even larger.

The second prediction that results from assuming that Mimas produced the observed signature concerns the characteristics of the electron spectrum necessary to produce a localized signature. The radial width of the observed signature was $\Delta L \sim 0.02$ or ~ 1200 km. At this position in its orbit, near its maximum radial excursion, Mimas traverses this distance in ~ 2 hours. Thus if Mimas had produced this signature, all of the electrons that were absorbed to form the signature must have been absorbed within ~ 2 hours, that is, across the signature the age varied by only ~ 2 hours. Since this was the only signature observed outbound, all of the electrons in this region must have been confined to an energy range that was narrow enough so that the hole age varied by only ~ 2 hours over that range. This constraint on the width of the electron spectrum becomes particularly severe near the resonance energy of ~ 1.1 MeV. Alternatively, if another satellite is assumed which is nearer the outbound position of the spacecraft, then the hole age plotted

in Fig. 5 is reduced by a factor that is roughly the ratio of the longitude differences from Voyager of the presumed satellite and of Mimas. If, for example, the new satellite were 20° from the outbound position of Voyager, then for the outbound curve of Fig. 5 the age scale should be multiplied by ~ 0.1 . In this case a 2-hour variation in hole age would cover all energies except very near the resonance. Thus a broad energy spectrum can easily be accommodated by assuming the existence of another satellite.

Information on the character of the electron spectrum in this region can be obtained from the double minimum structure evident in the BS4 rate displayed in Fig. 4B. This double minimum probably results from the response characteristics of the BS4 rate. The BS4 rate is a coincidence rate between two detectors (B2 and C4) with nominal energy thresholds of 2.2 MeV (B2) and 5.3 MeV (C4). During the period displayed in Fig. 4 this rate included accidental coincidences between these two detectors (which produce a rate proportional to the product of the single detector counting rates) as well as any true coincidences. The first minimum, which occurred 100 to 110 seconds before the minimum observed simultaneously in the B2 singles rate (and other rates with thresholds below 2 MeV), is thus probably due to a minimum in the C4 rate which has a higher nominal energy threshold. Since the absorption signature is different in the counting rates of detectors with different energy thresholds, the ambient electron flux must be distributed over a broad energy range. Thus our data are inconsistent with a monoenergetic electron spectrum.

A microabsorption signature was also observed within the orbital range of Mimas by charged particle detectors on the Pioneer 11 spacecraft when Mimas was $\sim 60^\circ$ east of Pioneer 11. Van Allen *et al.* (11) attributed that signature to Mimas, and concluded that the electron spectrum was sharply peaked at 1.6 MeV. The absorption signature observed on Pioneer 11 would have had an age of 6.44 hours if it were due to the absorption of electrons by Mimas (11). From this age and the characteristics of the signature, Van Allen *et al.* (11) estimated that the width of the electron spectrum was ≤ 0.1 MeV. For these Voyager 2 observations, however, the 1.6-MeV absorption signature due to Mimas would have been ~ 30 hours old. Thus the constraints on the width of the electron spectrum necessary to obtain a localized absorption signature for the Voyager 2 observations would be more severe than

Table 1. Positions of magnetospheric absorption features.

Name of feature	Expected position L	Observed position			
		Inbound		Outbound	
		L	λ^* (degrees)	L	λ^* (degrees)
Mimas I [†]	3.02	3.07	19	3.00	-4
Mimas O [†]	3.14	3.19	21	3.12	-6
Enceladus	3.95	4.00	27	3.91	-14
Tethys	4.89			4.80	-19

*Spacecraft latitude measured from Saturn's equatorial plane.

[†]I and O refer to the inner and outer edges of the Mimas absorption region.

they were in the Pioneer 11 case, and, as argued above, a similar signature should have been observed inbound. Thus the interpretation of Van Allen *et al.* (11) does not satisfy our observations. However, Simpson *et al.* (9) interpreted the Pioneer 11 signature as evidence for additional material at a trailing Lagrangian point in Mimas' orbit. The object that is inferred from the analysis presented here, we suggest, must have been at a longitude roughly on the opposite side of Saturn from Mimas near the time the Voyager signature was observed. Thus either we have seen an absorption signature due to an additional satellite, or, if it is the same object, it shares the orbit of Mimas but is not phase-locked in longitude to Mimas.

Magnetic field geometry. The absorption signatures of the satellites and rings of Saturn provide information not only on the existence of these absorbers and the dynamics of the charged-particle flux distributions, but also on the geometry of

the magnetic field, since charged particles closely follow magnetic field lines during their latitudinal bounce motion. The trajectory of Voyager 2 with its high latitude passage through the inner magnetosphere provides a particularly sensitive measure of any tilt of the internal magnetic dipole relative to Saturn's axis of rotation or any north-south offset of the center of the equivalent dipole.

Using a model of Saturn's internal magnetic field which consists of a centered dipole aligned with Saturn's rotation axis, we find significant deviations between the expected and observed positions of the various absorption features observed in the inner magnetosphere (Table 1). A striking example of this deviation is shown in Fig. 6 which illustrates the microabsorption signature observed at Tethys. Similarly, on the assumption of a centered dipole aligned with Saturn's rotation axis, the high-energy proton minimum at Enceladus and at the inner and outer edges of the

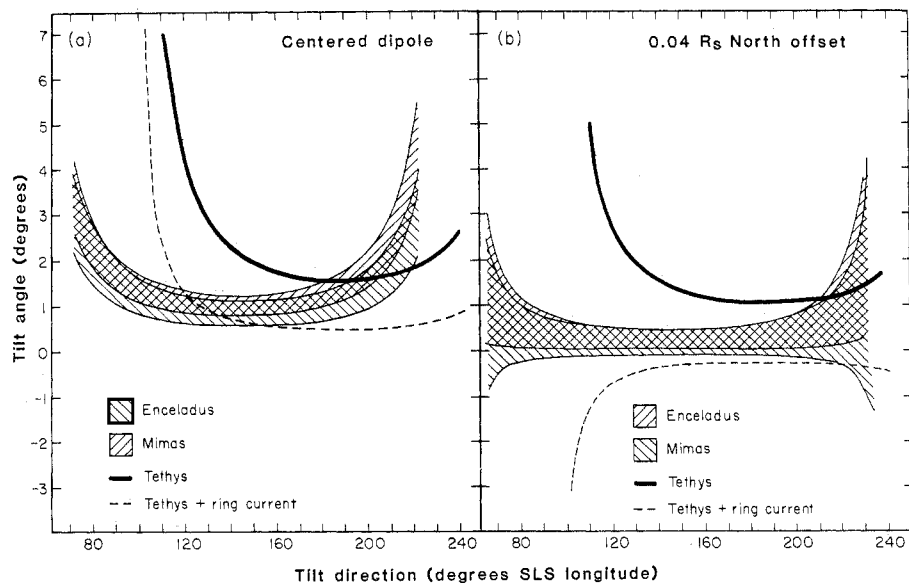


Fig. 7. The orientation of Saturn's magnetic dipole required to account for the observed positions of the absorption features at Enceladus, Mimas, and Tethys. Two positions were assumed for the dipole: (a) Saturn-centered, and (b) offset $0.04 R_S$ north. The cross-hatched bands indicate the range of values consistent with the uncertainties in the positions of the Mimas and Enceladus features. The corresponding uncertainty for Tethys is small. The dashed curve shows the result of including the effect of the Voyager 1 model ring current (8, 16) for the Tethys feature.

Mimas absorption region (Fig. 4, A and B) occur antisymmetrically at magnetic L coordinates which are larger than expected inbound, in the northern hemisphere, and smaller than expected outbound, in the southern hemisphere. Thus, on the basis of the energetic charged particle data, a simple centered dipole aligned with Saturn's rotation axis is not a satisfactory description of the magnetic field even in the inner magnetosphere. The deviations observed require a modification of the field from the centered, untilted model which is antisymmetric between the northern and southern hemispheres, thus suggesting a north-south offset of the dipole center, or, since our data cover a narrow longitude range, a tilt of the dipole. An equatorial ring current would produce a distortion which is symmetric between the northern and southern hemispheres, and thus cannot account for these observations.

Models of Saturn's magnetic field obtained from analyses of magnetometer data on the Pioneer 11 (13) and the Voyager 1 (14) spacecraft indicate that the internal field is dipolar. These models have also suggested that the dipole may be slightly tilted relative to Saturn's rotation axis or offset along that axis from the center of the planet. Accordingly, we have reanalyzed our data to determine the tilt and offset which are consistent with the positions of the absorption features that we observed in the inner magnetosphere. In this analysis (based on the predicted spacecraft trajectory) two positions for the dipole were considered: planet-centered and offset $0.04 R_S$ north. At each of these positions the dipole tilt required to align our observations inbound and outbound was calculated as a function of the longitude direction of the tilt. The results of this analysis (Fig. 7, a and b) indicate that if the dipole were centered on Saturn, the orientation that provides the best description of our data has a tilt of $\sim 1^\circ$ toward longitude (SLS) of 120° to 200° . Alternatively, if the dipole were offset $0.04 R_S$ north as suggested by Smith *et al.* (13), our data are consistent with no tilt ($< 0.5^\circ$), provided that a ring current is included in the model for the Tethys observation (15, 16).

These observations are biased, however, since all were obtained over a narrow range of Saturn longitudes (-45° to $+8^\circ$ SLS). Thus these data are less sensitive to any component of the tilt normal to the direction from Saturn to the spacecraft, that is, toward SLS longitudes of 45° to 100° and 225° to 280° . In addition, the nondipolar distortions in-

duced by currents in Saturn's magnetosphere (15), which may be expected to have the greatest effect in these data at Tethys, have only crudely been taken into account. With these caveats, our results are inconsistent with the 0.7° to 1.77° dipole tilt toward 324° to 352° SLS deduced from Voyager 1 magnetometer observations (14), since for a centered dipole our results suggest a tilt of this magnitude toward the opposite hemisphere.

The most recent, but preliminary, Saturnian magnetic field analysis, obtained by combining Voyager 1 vector and Voyager 2 magnitude data (3), yields a centered dipole tilted by 0.8° toward 280° SLS (equivalent to -0.8° toward 100° in Fig. 7, a and b). For this dipole orientation our results suggest a significant northward offset of the dipole ($> 0.04 R_S$). Clearly, a definitive determination of the structure of Saturn's magnetic field will require a synthesis of these data with the magnetometer observations and must include better estimates of the effects of any current systems operating within Saturn's magnetosphere.

R. E. VOGT
D. L. CHENETTE
A. C. CUMMINGS
T. L. GARRARD
E. C. STONE

California Institute of Technology,
Pasadena 91125

A. W. SCHARDT
J. H. TRAINOR
N. LAL
F. B. McDONALD

NASA Goddard Space Flight Center,
Greenbelt, Maryland 20771

References and Notes

1. For a description of the cosmic-ray system on the Voyager 1 and 2 spacecraft, see E. C. Stone, R. E. Vogt, F. B. McDonald, B. J. Teegarden, J. H. Trainor, J. R. Jokipii, W. R. Webber, *Space Sci. Rev.* **21**, 355 (1977).
2. H. S. Bridge *et al.*, *Science* **215**, 563 (1982).
3. N. F. Ness, M. H. Acuña, K. W. Behannon, L. F. Burlaga, J. E. P. Connerney, R. P. Lepping, F. M. Neubauer, *ibid.*, p. 558.
4. R. E. Vogt, D. L. Chenette, A. C. Cummings, T. L. Garrard, E. C. Stone, A. W. Schardt, J. H. Trainor, N. Lal, F. B. McDonald, *ibid.* **212**, 231 (1981).
5. N. F. Ness, personal communication.
6. We define L as $R/\cos^2(\lambda)$, where R is the radial distance from Saturn in Saturn radii (the radius of Saturn is taken to be 60,330 km), and λ is the magnetic latitude.
7. F. B. McDonald, A. W. Schardt, J. H. Trainor, *J. Geophys. Res.* **85**, 5813 (1980).
8. W. Fillius and C. McIlwain, *ibid.*, p. 5803.
9. J. A. Simpson, T. S. Bastian, D. L. Chenette, R. B. McKibben, K. R. Pyle, *ibid.*, p. 5731.
10. J. A. Van Allen, B. A. Randall, M. F. Thomsen, *ibid.*, p. 5679.
11. J. A. Van Allen, M. F. Thomsen, B. A. Randall, *ibid.*, p. 5709.
12. The Saturn longitude system, SLS, used in this report is a Saturn-fixed system with longitude increasing to the west [see M. D. Desch and M. L. Kaiser, *Geophys. Res. Lett.* **8**, 253 (1981)].
13. E. J. Smith *et al.*, *J. Geophys. Res.* **85**, 5655 (1980).
14. M. H. Acuña, J. E. P. Connerney, N. F. Ness, *Nature (London)* **292**, 721 (1981).
15. J. E. P. Connerney, M. H. Acuña, N. F. Ness, *ibid.*, p. 724.
16. J. E. P. Connerney, personal communication.
17. Counting rates in this report were obtained from the following detectors of the cosmic-ray instrument: (≥ 0.43 -MeV protons) L1, $2.8 \text{ cm}^2 \times 35 \mu\text{m}$, 0.2-MeV threshold; (0.14- to 0.4-MeV electrons) A1, $8 \text{ cm}^2 \times 0.15 \text{ mm}$, 0.1-MeV threshold; (≥ 0.35 -MeV electrons) B1, high gain, $8 \text{ cm}^2 \times 2 \text{ mm}$, 0.3-MeV threshold; (1- to 2-MeV electrons) B1, low gain, $8 \text{ cm}^2 \times 2 \text{ mm}$, 1.0-MeV threshold; (> 2.5 -MeV electrons) B2, low gain, $8 \text{ cm}^2 \times 2 \text{ mm}$, 2.2-MeV threshold; (> 0.6 -MeV electrons) D1, $4.5 \text{ cm}^2 \times 3 \text{ mm}$, 0.5-MeV threshold. See (1) for more information.
18. We thank the Voyager project members and the enthusiastic staff of our laboratories at Caltech and Goddard Space Flight Center for their splendid support. Special thanks go to W. Alt-house, M. Fernandez, R. Kelly, and I. Matus (Caltech), W. Davis, H. Domchick, and D. Stillwell (Goddard), and O. Divers, E. Franzgrote, and R. Parker (Jet Propulsion Laboratory). Supported by NASA under NAS7-100 and NGR 05-002-160.

10 November 1981

Planetary Radio Astronomy Observations from Voyager 2 Near Saturn

Abstract. *Planetary radio astronomy measurements obtained by Voyager 2 near Saturn have added further evidence that Saturnian kilometric radiation is emitted by a strong dayside source at auroral latitudes in the northern hemisphere and by a weaker source at complementary latitudes in the southern hemisphere. These emissions are variable because of Saturn's rotation and, on longer time scales, probably because of influences of the solar wind and Dione. The electrostatic discharge bursts first discovered by Voyager 1 and attributed to emissions from the B ring were again observed with the same broadband spectral properties and an episodic recurrence period of about 10 hours, but their occurrence frequency was only about 30 percent of that detected by Voyager 1. While crossing the ring plane at a distance of 2.88 Saturn radii, the spacecraft detected an intense noise event extending to above 1 megahertz and lasting about 150 seconds. The event is interpreted to be a consequence of the impact, vaporization, and ionization of charged, micrometer-size G ring particles distributed over a vertical thickness of about 1500 kilometers.*

The Voyager 2 planetary radio astronomy (PRA) instrument (1) made observations of several radio wave phenomena

during the encounter with Saturn on 26 August 1981. We describe here three of the phenomena: Saturn kilometric radia-